

Distributed Noise-resilient Networked Synchrony of Active Distribution Systems

Shankar Abhinav, *Graduate Student Member, IEEE*, Ioannis D. Schizas, *Member, IEEE*
 Frank L. Lewis, *Fellow, IEEE*, and Ali Davoudi, *Senior Member, IEEE*

Abstract—This paper proposes a distributed noise resilient control technique for voltage and frequency synchronization in inverter-based AC microgrids. Existing cooperative control techniques assume ideal communication among inverters. The effect of additive noise in communication links among inverters, and between the reference signal and inverters, on the synchronization process, is studied. Distributed least mean-square solutions estimate the reference set points, and a local least mean-square algorithm estimates neighboring inverter frequencies and voltages. The efficacy of the proposed solution, for an islanded microgrid test system under the additive noise in reference communication links and links connecting neighboring inverters, is evaluated for a modified IEEE 34-bus feeder system. An upper bound for the noise-induced deviation in the consensus parameter is analytically derived and verified by the simulated testbed.

Index Terms—AC microgrids, cooperative control, distributed control, distributed estimation, noise, secondary control.

NOMENCLATURE

\mathbf{A}	Adjacency matrix of the communication graph.
\mathbf{L}	Laplacian matrix of the communication graph.
g_i	Pinning gain associate with inverter i .
\mathbf{G}	Diagonal matrix of pinning gains.
\mathbf{x}_i	State vector for dynamics of inverter i .
ω_i	Output frequency of inverter i .
V_i	Output voltage of inverter i .
ω_{ref}	Reference frequency.
v_{ref}	Reference voltage.
ω_{ni}	Frequency set point in droop control of inverter i .
V_{ni}	Voltage set point in droop control of inverter i .
e_{vi}	Voltage error term in cooperative secondary control for inverter i .
e_{ω_i}	Voltage error term in cooperative secondary control for inverter i .
r_{ref_i}	Noise in link between reference and inverter i .
r_{ij}	Noise in link between inverter i and inverter j .
$\bar{\omega}_{\text{ref},i}$	Local estimate of reference frequency at inverter i .
$\bar{\omega}_j$	Local estimate of inverter j frequency at inverter i .
\mathbf{R}_i	Noise parameter associated with the communication links in between inverters.

The work has been supported in part by the National Science Foundation under Grant ECCS-1405173, CCF-1218079, and by the U.S. Office of Naval Research under Grant N00014-14-1-0718.

Authors are with Electrical Engineering Department, the University of Texas at Arlington, TX 76019 USA (phone: 817-272-1374; fax: 817-272-2253; e-mail: (shankar.abhinav@mavs.uta.edu, schizas@uta.edu, lewis@uta.edu, and davoudi@uta.edu).

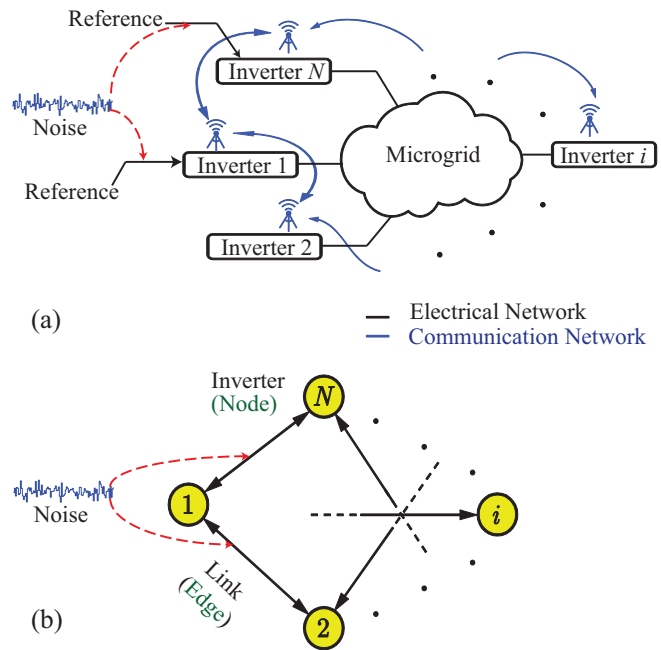


Fig. 1. Incorporating communication noise in distributed control of AC microgrids: a) Multi-inverter AC microgrids; b) Graphical representation of information exchange among inverters.

\mathbf{R}_o	Noise parameter associated with the communication links between inverters and the reference.
σ^2	Noise variance.

I. INTRODUCTION

Autonomous inverter-interfaced AC microgrids are finite-inertia power systems that are islanded (isolated) from the main grid. In a microgrid control hierarchy [1]–[3], the primary control maintains the inverter output voltage and frequency, usually through droop mechanisms at each inverter. The secondary control ensures synchrony of voltage and frequency variables among inverters by setting the set points for the primary control. The conventional centralized secondary control [4]–[6] requires point-to-point communication, exposes a single point-of-failure, and increases complexity. Alternatively, distributed control strategies are inspired by spatially-dispersed microgrids, and utilize a sparse communication network to exchange information among inverters [7]–[11], as seen in Fig. 1.

Existing distributed control paradigms assume an ideal, noise-free communication among inverters. In practice, the communication channels will be corrupted by additive noise

[12]. For example, in wireless communications, an additive noise will be generated in the receiver front end and surrounding noise picked up by the antenna. Environmental causes, e.g., rain, can also introduce noise in to communication channels. The additive noise associated with electronic components and amplifiers at the receiver end is classified as thermal noise and statistically modeled as Gaussian in nature [12]. Without loss of generality, in this paper, noise is considered to be zero mean white Gaussian. Consensus on the desired set point is not warranted in the presence of noise [13]. Noise could especially disrupt the frequency synchronization. Given the nominal threshold of ± 0.05 Hz on frequency deviation [14], small deviation can adversely affect the sensitive electronics loads, while larger deviations can lead to circulating currents and, can potentially, destabilize the microgrid.

The effect of noise and distributed estimators for a noisy multi-agent system have been studied in [15], [16]. ADMM is an iterative algorithm to solve convex minimization problems that combines decomposability of dual descent with the faster convergence property of the method of multipliers. The distributed least mean-squares algorithm (DLMS) method is adopted in this paper in contrast to other distributed estimation approaches [17], [18], as it offers robustness and fast convergence rates, and relies on a single-hop communication among agents [19], [20]. The initial work of the authors in [21] had considered the communication noise only in the reference signal linked to the leader inverter (i.e., the pinned reference link). This paper generalizes the concept and considers additive communication noise in all the communication links among all inverters. The effect of additive communication noise is reduced by incorporating a distributed estimation technique in secondary cooperative control. It uses the same communication topology employed in the cooperative control for decentralized estimation in the presence of noisy data. The DLMS algorithm is used to estimate the reference set points, and a local LMS algorithm estimates the neighboring inverter frequency and voltage.

This paper is organized as follows. Section II provides preliminaries of graph theory. Cooperative control of inverter-based microgrid are presented in Section III. In Section IV, a distributed scheme estimates the reference and neighbor's signals corrupted with an additive noise. An upper bound on the noise-induced deviation from the consensus value is obtained in section V. Case studies, using a 34-bus IEEE feeder network augmented with six inverters, are presented in Section VI. The conclusion is drawn in Section VII.

II. PRELIMINARY OF GRAPH THEORY

The communication network among inverters $1, 2, \dots, N$ is represented by a graph $Gr = (O, E)$, as shown in Fig. 1(b). $O = \{o_1, o_2, \dots, o_n\}$ is a set of n nodes or vertices corresponding to each inverter. E is a set of edges or arcs, where each edge from o_i to o_j is denoted by (o_i, o_j) . N_i is the set of inverters providing information to inverter i , also referred to as its neighbors. The graph can be represented by an adjacency matrix $\mathbf{A} = [a_{ij}]$, with weights $a_{ij} > 0$ if $(o_i, o_j) \in E$, otherwise $a_{ij} = 0$. The diagonal in-degree matrix is defined as $\mathbf{D} = \text{diag}\{N_i\}$.

The graph Laplacian matrix, $\mathbf{L} = \mathbf{D} - \mathbf{A}$, includes distributed system properties, e.g., the convergence rate. A path from node i to node j is a sequence of edges $(o_i, o_k), (o_k, o_l), \dots, (o_m, o_j)$. A graph is said to have a spanning tree, if there is a root node with a path from that node to every other node in the graph. If a graph has a spanning tree which implies that the communication graph is connected, the Laplacian matrix eigenvalue $\lambda_1 = 0$ is a simple eigenvalue [22]. The solution to $\mathbf{L}\omega = \mathbf{0}$ can be written as $\omega = c\mathbf{1}$, where c is a constant. Thus, synchronization is guaranteed as long as the communication graph has a spanning tree.

A leader node can be connected to some nodes (at least to one root node) by unidirectional edges. The nodes connected to the leader node and the corresponding connecting edges are called pinned nodes and pinning edges, respectively. A gain is assigned to each pinning edge, e.g., g_i is the pinning gain from the leader to the node i . The pinning gain is zero for an unpinned node. The pinning gain matrix is $\mathbf{G} = \text{diag}\{g_i\}$.

III. COOPERATIVE CONTROL OF AC MICROGRIDS

A. Dynamic Modeling of Inverters

In this section, the nonlinear large-signal inverter model is explored. Moreover, preliminaries of cooperative control strategy for the secondary control of AC microgrids is presented, assuming ideal communication among inverters. This drawback is addressed in the next section. Figure 2 shows the block diagram of inverter-based AC microgrids. The dynamics of DC bus voltage and switching harmonics are usually neglected [23], [24]. The large-signal dynamical model of an inverter, with internal control loops, is adopted from [24]

$$\begin{cases} \frac{dx_i}{dt} = f_i(x_i) + g(x_i)u_i \\ y_i = h_i(x_i) \end{cases}, \quad (1)$$

where the state vector is

$$\mathbf{x}_i = [\delta_i, P_i, Q_i, \phi_{di}, \phi_{qi}, \gamma_{di}, \gamma_{qi}, i_{ldi}, i_{lqi}, v_{odi}, v_{oqi}, i_{odi}, i_{oqi}]. \quad (2)$$

The reference frame of one inverter is considered as the common reference frame ω_{com} . The angle of other inverters, ω , is found from

$$\frac{d\delta_i}{dt} = \omega - \omega_{\text{com}}. \quad (3)$$

The inductive load dynamics are modeled as

$$\begin{cases} \frac{di_{load,d}}{dt} = -\frac{R_{load}}{L_{load}}i_{load,d} + \omega i_{load,q} + \frac{1}{L_{load}}v_{bd} \\ \frac{di_{load,q}}{dt} = -\frac{R_{load}}{L_{load}}i_{load,q} - \omega i_{load,d} + \frac{1}{L_{load}}v_{bq} \end{cases}. \quad (4)$$

The equations (1)-(3) represent the dynamic modeling of the inverter and inductive loads used for analysis and simulation purposes.

B. Cooperative Control of AC Microgrids

Decentralized droop techniques are conventionally employed for the primary control assuming inductive power distribution networks

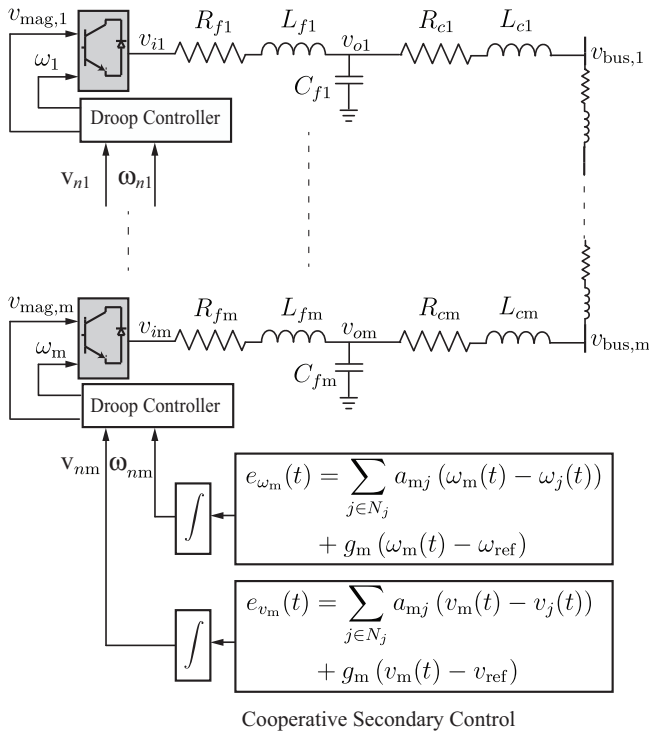


Fig. 2. Cooperative control of inverter-based microgrids.

$$\begin{cases} \omega_i = \omega_{ni} - m_{pi}P_i \\ v_{mag,i} = V_{ni} - n_{qi}Q_i \end{cases}, \quad (5)$$

where $v_{mag,i}$ and ω_i are the reference voltage and frequency provided for the internal control loops. ω_{ni} and V_{ni} are the set points for the primary control in (5). P_i and Q_i are the inverters' active and reactive powers. m_{pi} and n_{qi} are the droop coefficients evaluated based on the inverter ratings.

The secondary control provides ω_{ni} and V_{ni} in (5), to synchronize the terminal voltages and frequencies of each inverter to the reference values. This can be achieved by each inverter exchanging data only with its neighbors on a communication graph. The voltage error term is obtained by cooperation among inverters based on [9], [24] to update V_{ni}

$$e_{vi}(t) = \sum_{j \in N_i} (v_i(t) - v_j(t)) + g_i (v_i(t) - v_{ref}), \quad (6)$$

where v_i and v_j are the voltages of the inverters i and j , neighboring on the graph. To ensure consensus, some inverters are pinned with reference values. The pinning gain $g_i \geq 0$ is the weight of the edge connecting inverter i with the reference v_{ref} . Likewise, the cooperative frequency control law to update ω_{ni} based on [9], [24] is

$$e_{\omega_i}(t) = \sum_{j \in N_i} (\omega_i(t) - \omega_j(t)) + g_i (\omega_i(t) - \omega_{ref}), \quad (7)$$

where ω_i and ω_j are the frequencies of inverters i and j on the graph. The pinning gain is non-zero for the inverters connected to the reference frequency ω_{ref} . The overall block diagram of the distributed cooperative control is shown in Fig. 2. This cooperative secondary control ensures synchronization of inverter frequencies and output voltages to the

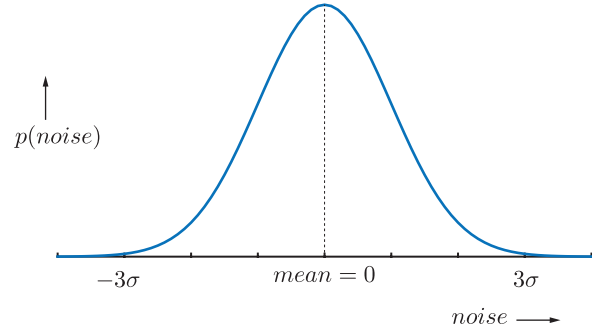


Fig. 3. Probability distribution function of noise (white gaussian).

reference set points, but assumes ideal communication and neglects the inevitable presence of noise in the communication channels.

IV. DISTRIBUTED NOISE REDUCTION

In this section, a fully distributed approach is proposed to estimate parameters communicated for the secondary control between the neighboring inverters, as well as the pinned inverters and the reference signals.

A. Communication Noise

The pinning and communication links among inverters are assumed to be corrupted by noise that is zero-mean Gaussian. The probability distribution function of this noise signal with variance σ^2 is shown in Fig. 3 and given by

$$p(noise) = \frac{1}{\sqrt{2\pi\sigma^2}} \exp\left(-\frac{noise^2}{2\sigma^2}\right). \quad (8)$$

The proposed algorithm is general and not restricted by the noise type. However, to streamline the analytics, the noise is considered to be zero-mean. Otherwise, methods such as sample averaging [25] can render the noise zero mean. The links between the pinned inverter i and the leader node has a zero-mean additive noise $r_{ref,i}(t)$, with a covariance $C_{r_o} := E[r_{ref,i}(t)r_{ref,i}(t)^T]$, received at inverter i . The corrupted reference frequency and voltage signals for the pinned inverters are

$$\begin{cases} \omega_{ref,i}(t) = \omega_{ref} + r_{ref,i}(t) \\ v_{ref,i}(t) = v_{ref} + r_{ref,i}(t). \end{cases} \quad (9)$$

The communication links among inverters have a zero-mean additive noise $r_{ij}(t)$, with a covariance $C_{r_{ij}} := E[r_{ij}(t)r_{ij}(t)^T]$, received at the inverter j from the inverter i . The corrupted reference frequency and voltage signals are

$$\begin{cases} \omega_{ij}(t) = \omega_i + r_{ij}(t) \\ v_{ij}(t) = v_i + r_{ij}(t). \end{cases} \quad (10)$$

B. Signal Estimation Under Noisy Communications

In presence of communication noise, synchronization of voltage and frequency terms might not be properly achieved. Fully-distributed estimation techniques [19], [20] are modified

to address the presence of additive noise. The presence of noise in communicated frequency terms is considered; the same discussion can be extended to the voltage terms. The frequency reference set point is communicated to pinned inverters. These local reference set points $\omega_{\text{ref},1}, \omega_{\text{ref},2}, \dots, \omega_{\text{ref},N}$ are corrupted by the additive noise. For synchronization of inverter frequencies, it is necessary to estimate the reference frequency set points from the corrupted local frequency set points using a LMS estimator. The centralized LMS estimator is given by

$$\begin{aligned} \hat{\omega}_{\text{ref}}(t) &= \arg \min_{\bar{\omega}_{\text{ref}}} \mathbb{E}[\|\omega_{\text{ref}}(t) - \bar{\omega}_{\text{ref}}\|^2] \\ &= \arg \min_{\bar{\omega}_{\text{ref}}} \sum_{i=1}^N \mathbb{E}[(\omega_{\text{ref},i}(t) - \bar{\omega}_{\text{ref}})^2], \end{aligned} \quad (11)$$

where $\mathbb{E}[\|\omega_{\text{ref}}(t) - \bar{\omega}_{\text{ref}}\|^2]$ is the estimate of the mean-square error. The distorted and estimated reference frequencies are denoted by $\omega_{\text{ref}}(t)$ and $\bar{\omega}_{\text{ref}}$, respectively.

A distributed solution can be formulated, using local optimization and distributed implementation of (11). The global variable $\bar{\omega}_{\text{ref}}$ is replaced by its local estimates $\bar{\omega}_{\text{ref},1}, \bar{\omega}_{\text{ref},2}, \dots, \bar{\omega}_{\text{ref},N}$. A separable formulation, that adheres to the communication graph connectivity, is

$$\begin{aligned} \{\hat{\omega}_{\text{ref},i}(t)\}_{i=1}^N &= \arg \min_{\bar{\omega}_{\text{ref},i}} \sum_{i=1}^N \mathbb{E}[(\omega_{\text{ref},i}(t) - \bar{\omega}_{\text{ref},i})^2] \\ &\text{subject to } \bar{\omega}_{\text{ref},i} = \bar{\omega}_{\text{ref},j}, i \in N, j \in N_i \end{aligned} \quad (12)$$

where $\bar{\omega}_{\text{ref},i}$ and $\bar{\omega}_{\text{ref},j}$ are the local estimates of reference frequency at inverters i and j , respectively. If the communication graph is connected, the constraints $\bar{\omega}_{\text{ref},i} = \bar{\omega}_{\text{ref},j}$ in (12) impose consensus on the local reference frequency estimates. We solve (12) in a distributed manner using the Alternating Direction Method of Multipliers (ADMM) [26]. To facilitate application of ADMM, auxiliary variables s replace the constraints in (12) with

$$\bar{\omega}_{\text{ref},i} = s_i; \bar{\omega}_{\text{ref},j} = s_j, i \in N, j \in N_i \quad (13)$$

Lagrange multipliers $[a, b] := a_i^j, b_i^j$, and the auxiliary variables, are used to form a quadratic Lagrangian function

$$\begin{aligned} \mathcal{L}[\bar{\omega}_{\text{ref}}, s, a, b] &= \sum_{i=1}^N \mathbb{E}[(\omega_{\text{ref},i}(t) - \bar{\omega}_{\text{ref},i})^2] \\ &+ \sum_{i=1}^N \sum_{j \in N_i} \left[(a_i^j)^T (\bar{\omega}_{\text{ref},i} - s_i) + (b_i^j)^T (\bar{\omega}_{\text{ref},i} - s_j) \right] \\ &+ \sum_{i=1}^N \sum_{j \in N_i} \frac{c}{2} [\|\bar{\omega}_{\text{ref},i} - s_i\|^2 + \|\bar{\omega}_{\text{ref},i} - s_j\|^2], \end{aligned} \quad (14)$$

where $c > 0$ is a penalty coefficient.

ADMM is an iterative process that updates the multipliers, local frequency estimates, and auxiliary variables at each time instant. It has been shown in [20] that auxiliary variables can be eliminated. The ADMM results in two updates of the Lagrange multipliers and the local reference frequency estimate, (15) and (16), at each time instant. Lagrange multipliers are

$$a_i^j(t) = a_i^j(t-1) + \frac{c}{2} (\bar{\omega}_{\text{ref},i}(t) - \bar{\omega}_{\text{ref},j}(t)). \quad (15)$$

The local reference frequency estimate, $\bar{\omega}_{\text{ref},i}$, is

$$\begin{aligned} \bar{\omega}_{\text{ref},i}(t+1) &= \arg \min_{\bar{\omega}_{\text{ref},i}} \mathbb{E}[(\omega_{\text{ref},i}(t) - \bar{\omega}_{\text{ref},i})^2] \\ &+ \sum_{j \in N_j} \left(a_i^j(t) - a_j^i(t) \right) \bar{\omega}_{\text{ref},i} \\ &+ c \sum_{j \in N_j} \left\| \bar{\omega}_{\text{ref},i}(t) - \frac{1}{2} (\bar{\omega}_{\text{ref},i}(t) + \bar{\omega}_{\text{ref},j}(t)) \right\|^2. \end{aligned} \quad (16)$$

The update of local reference frequency estimate, for every recursion, is

$$\begin{aligned} \bar{\omega}_{\text{ref},i}(t+1) &= \bar{\omega}_{\text{ref},i}(t) + \mu [2(\omega_{\text{ref},i}(t+1) - \bar{\omega}_{\text{ref},i}(t)) \\ &- \sum_{j \in N_j} (a_i^j(t) - a_j^i(t)) \\ &- c \sum_{j \in N_j} (\bar{\omega}_{\text{ref},i}(t) - \bar{\omega}_{\text{ref},j}(t))] \end{aligned} \quad (17)$$

where μ is the update step-size. The noise can be accounted for by incorporating communication noise η_i^j and $\bar{\eta}_i^j$, which corrupts the Lagrange multipliers and the local reference frequency estimates of the neighboring inverter, respectively. The Lagrange multiplier and local reference frequency estimate, in presence of communication noise, are given by (18), (19).

$$a_i^j(t) = a_i^j(t-1) + \frac{c}{2} \left(\bar{\omega}_{\text{ref},i}(t) - (\bar{\omega}_{\text{ref},j}(t) + \eta_i^j) \right) \quad (18)$$

$$\begin{aligned} \bar{\omega}_{\text{ref},i}(t+1) &= \bar{\omega}_{\text{ref},i}(t) + \mu [2(\omega_{\text{ref},i}(t+1) - \bar{\omega}_{\text{ref},i}(t)) \\ &- \sum_{j \in N_j} (a_i^j(t) - (a_j^i(t) + \bar{\eta}_i^j)) \\ &- c \sum_{j \in N_j} (\bar{\omega}_{\text{ref},i}(t) - (\bar{\omega}_{\text{ref},j}(t) + \eta_i^j))]. \end{aligned} \quad (19)$$

The DLMS algorithm to estimate the reference frequency has to find the local Lagrange multiplier using (18), and update the local reference frequency estimate using (19). Each inverter communicates its reference frequency estimate and the Lagrange multiplier to its neighbors. The stability of DLMS algorithm has been studied in [20]. The local frequencies communicated to neighbors are corrupted due to the presence of noise in the neighboring communication links. A local LMS algorithm can estimate the frequencies of neighboring inverters at each inverter i . The distorted and estimated inverter

Algorithm 1 Secondary Control Augmented with Estimation

Initialize $a_i^j(-1)$ and $\bar{\omega}_{\text{ref},i}$

for $t = 0, 1, \dots$ **do**

 Transmit $\bar{\omega}_{\text{ref},i}(t)$ and $\omega_i(t)$ to neighbors

 Update $a_i^j(t)$ using (18)

 Transmit $a_i^j(t)$ to neighbors

 Update $\bar{\omega}_{\text{ref},i}(t+1)$ using (19)

 Estimate $\bar{\omega}_j(t+1)$ using (21)

 Update $\omega_i(t+2)$ by substituting $\bar{\omega}_{\text{ref},i}(t+1)$ and $\bar{\omega}_j(t+1)$ in place of $\omega_{\text{ref}}(t)$ and $\omega_j(t)$ in (7)

end for

frequencies are denoted by $\omega_j(t)$ and $\bar{\omega}_j$, respectively. The LMS estimator at every inverter i for the neighboring inverters $j \in N_i$ frequencies is obtained by minimizing

$$\hat{\omega}_j(t) = \arg \min_{\bar{\omega}_j} E[|\omega_j(t) - \bar{\omega}_j|^2] \quad \forall j \in N_i, \quad (20)$$

where $E[|\omega_j(t) - \bar{\omega}_j|]$ is the mean-square error. The frequency estimate update, for every recursion, is

$$\bar{\omega}_j(t+1) = \bar{\omega}_j(t) + \mu(\omega_j(t+1) - \bar{\omega}_j(t)), \quad (21)$$

where μ is the step size for the updates. This approach is detailed in Algorithm 1. A similar algorithm can be used in tandem for the secondary control of inverter voltages.

V. NOISE-INDUCED BOUND ON FREQUENCY DEVIATION

To assess the robustness of the proposed method to additive noise levels in communication links, an upper error bound, on the deviation of local frequency estimates from their reference values, is derived. The error bound has been analytically derived a priori, to provide designer and operator with knowledge about the effect of noise prior to controller implementation and microgrid deployment. As a metric to measure error, we consider the mean-square error, $E[|\omega(t) - \omega_{\text{ref}}|^2]$, a standard performance index used in estimation.

The secondary cooperative frequency control, under additive noise in communication (and pinned reference) links, is

$$\dot{\omega}_i(t) = \sum_{j \in N_i} a_{ij} (\omega'_{ji}(t) - \omega_i(t)) + g_i (\omega'_{ref,i}(t) - \omega_i(t)), \quad (22)$$

where $\omega'_{ji}(t) = \omega_j(t) + r_{ji}(t)$ and $\omega'_{ref,i}(t) = \omega_{ref_0}(t) + r_{ref,i}(t)$. $\omega_j(t)$ is the frequency of inverter j , ω_{ref_0} is the reference frequency, and $r_{ji}(t)$ and $r_{ref,i}(t)$ are noise components. Expanding (22), one has

$$\begin{aligned} \dot{\omega}_i(t) &= \sum_{j \in N_i} a_{ij} (\omega_j(t) - \omega_i(t)) + g_i (\omega_{ref_0} - \omega_i(t)) \\ &+ \sum_{j \in N_i} a_{ij} r_{ji}(t) + g_i r_{ref,i}(t). \end{aligned} \quad (23)$$

This can be written in the vector form as

$$\dot{\omega}(t) = -(\mathbf{L} + \mathbf{G})(\omega(t) - \omega_{\text{ref}_0}) + \mathbf{R}_i(t) + \mathbf{R}_o(t), \quad (24)$$

where the graph Laplacian matrix is $\mathbf{L} = \mathbf{D} - \mathbf{A}$, and the diagonal matrix of pinning gains is $\mathbf{G} = \text{diag}(g_i)$. $\mathbf{R}_i = [a_{ij} \times r_{ji}(t)]$ and $\mathbf{R}_o = [g_i \times r_{ref,i}(t)]$ contain the noise parameters and their associated adjacency and pinned gains. The inverter frequencies, at time $t + \Delta t$, is

$$\begin{aligned} \omega(t + \Delta t) &= \omega(t) + \Delta t[-(\mathbf{L} + \mathbf{G})(\omega(t) - \omega_{\text{ref}_0}) \\ &+ \mathbf{R}_i(t) + \mathbf{R}_o(t)] \\ &= [\mathbf{I} - \Delta t(\mathbf{L} + \mathbf{G})] \omega(t) + \Delta t(\mathbf{L} + \mathbf{G}) \omega_{\text{ref}_0} \\ &+ \Delta t[\mathbf{R}_i(t) + \mathbf{R}_o(t)]. \end{aligned} \quad (25)$$

$$\begin{aligned} \|\mathbf{Error}(t + \Delta t)\|^2 &\leq \|(\mathbf{I} - \mathbf{T})^t \omega(0) + \sum_{k=0}^{t-1} (\mathbf{I} - \mathbf{T})^k \Delta t \mathbf{R}_o - \omega_{\text{ref}_0}\|^2 + \left\| \sum_{k=0}^{t-1} (\mathbf{I} - \mathbf{T})^k \Delta t \mathbf{R}_i(t - k\Delta t) \right\|^2 \\ &+ \left\| \sum_{k=0}^{t-1} (\mathbf{I} - \mathbf{T})^k \Delta t \mathbf{R}_o(t - k\Delta t) \right\|^2 + 2\left\| (\mathbf{I} - \mathbf{T})^t \omega(0) + \sum_{k=0}^{t-1} (\mathbf{I} - \mathbf{T})^k \Delta t \mathbf{R}_o - \omega_{\text{ref}_0} \right\| \\ &\left\| \sum_{k=0}^{t-1} (\mathbf{I} - \mathbf{T})^k \Delta t \mathbf{R}_i(t - k\Delta t) \right\| + 2\left\| (\mathbf{I} - \mathbf{T})^t \omega(0) + \sum_{k=0}^{t-1} (\mathbf{I} - \mathbf{T})^k \Delta t \mathbf{R}_o - \omega_{\text{ref}_0} \right\| \\ &\left\| \sum_{k=0}^{t-1} (\mathbf{I} - \mathbf{T})^k \Delta t \mathbf{R}_i(t - k\Delta t) \right\| + 2\left\| \sum_{k=0}^{t-1} (\mathbf{I} - \mathbf{T})^k \Delta t \mathbf{R}_i(t - k\Delta t) \right\| \\ &\left\| \sum_{k=0}^{t-1} (\mathbf{I} - \mathbf{T})^k \Delta t \mathbf{R}_o(t - k\Delta t) \right\| \end{aligned} \quad (26)$$

$$\begin{aligned} E[\|\mathbf{Error}(t + \Delta t)\|^2] &\leq \|(\mathbf{I} - \mathbf{T})^t \omega(0) + \sum_{k=0}^{t-1} (\mathbf{I} - \mathbf{T})^k \Delta t \mathbf{R}_o - \omega_{\text{ref}_0}\|^2 + \left\| \sum_{k=0}^{t-1} (\mathbf{I} - \mathbf{T})^k \Delta t \mathbf{R}_{i,\text{max}} \right\|^2 \\ &+ \left\| \sum_{k=0}^{t-1} (\mathbf{I} - \mathbf{T})^k \Delta t \mathbf{R}_{o,\text{max}} \right\|^2 + 2\left\| (\mathbf{I} - \mathbf{T})^t \omega(0) + \sum_{k=0}^{t-1} (\mathbf{I} - \mathbf{T})^k \Delta t \mathbf{R}_o - \omega_{\text{ref}_0} \right\| \\ &\left\| \sum_{k=0}^{t-1} (\mathbf{I} - \mathbf{T})^k \Delta t \mathbf{R}_{i,\text{max}} \right\| + 2\left\| (\mathbf{I} - \mathbf{T})^t \omega(0) + \sum_{k=0}^{t-1} (\mathbf{I} - \mathbf{T})^k \Delta t \mathbf{R}_o - \omega_{\text{ref}_0} \right\| \\ &\left\| \sum_{k=0}^{t-1} (\mathbf{I} - \mathbf{T})^k \Delta t \mathbf{R}_{o,\text{max}} \right\| + 2\left\| \sum_{k=0}^{t-1} (\mathbf{I} - \mathbf{T})^k \Delta t \mathbf{R}_{i,\text{max}} \right\| \left\| \sum_{k=0}^{t-1} (\mathbf{I} - \mathbf{T})^k \Delta t \mathbf{R}_{o,\text{max}} \right\| \end{aligned} \quad (27)$$

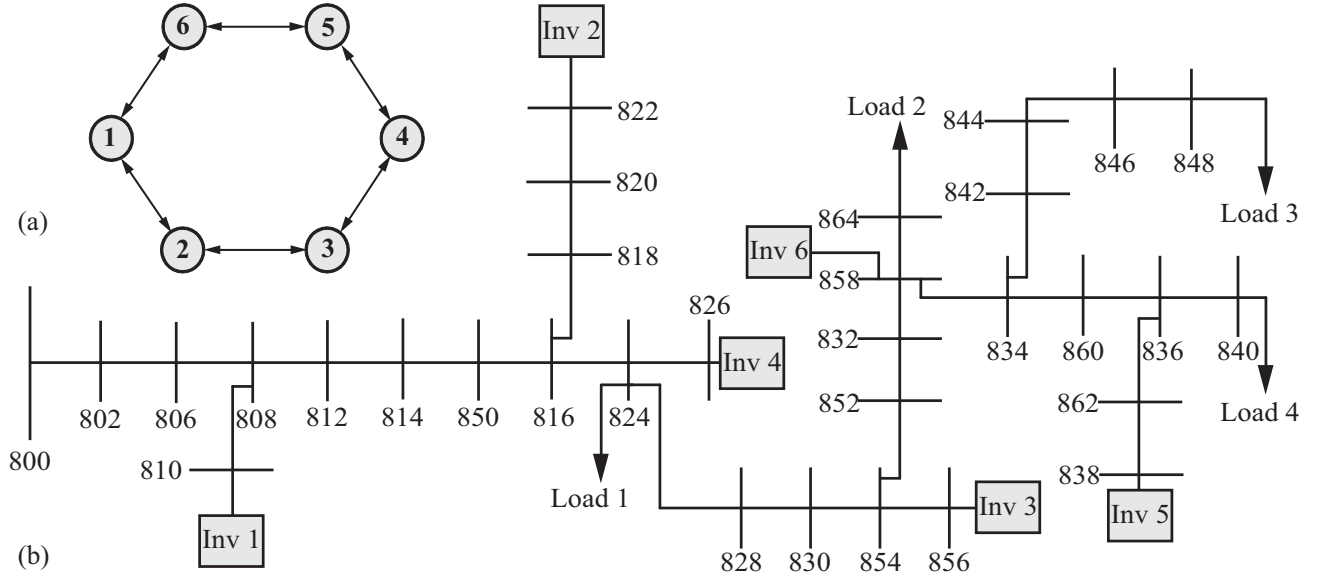


Fig. 4. (a) Topology of the communication network among inverters. (b) IEEE standard 34-bus feeder system augmented with six inverters.

To further simplify, let $\mathbf{T} = \Delta t (\mathbf{L} + \mathbf{G})$. By expanding (25), one has

$$\begin{aligned}
 \boldsymbol{\omega}(t + \Delta t) &= (\mathbf{I} - \mathbf{T}) \boldsymbol{\omega}(t) + \mathbf{T} \boldsymbol{\omega}_{\text{ref}0} + \Delta t [\mathbf{R}_i(t) + \mathbf{R}_o(t)] \\
 &= (\mathbf{I} - \mathbf{T})^2 \boldsymbol{\omega}_i(t - \Delta t) + (\mathbf{I} - \mathbf{T}) \mathbf{T} \boldsymbol{\omega}_{\text{ref}0} \\
 &\quad + (\mathbf{I} - \mathbf{T}) \Delta t [\mathbf{R}_i(t - \Delta t) + \mathbf{R}_o(t - \Delta t)] \\
 &\quad + \mathbf{T} \boldsymbol{\omega}_{\text{ref}0} + \Delta t [\mathbf{R}_i(t) + \mathbf{R}_o(t)] \\
 &= (\mathbf{I} - \mathbf{T})^t \boldsymbol{\omega}(0) + \sum_{k=0}^{t-1} (\mathbf{I} - \mathbf{T})^k \mathbf{T} \boldsymbol{\omega}_{\text{ref}0} \\
 &\quad + \sum_{k=0}^{t-1} (\mathbf{I} - \mathbf{T})^k \Delta t [\mathbf{R}_i(t - k\Delta t) + \mathbf{R}_o(t - k\Delta t)]. \quad (28)
 \end{aligned}$$

The control objective is to synchronize all the frequencies to the reference value. The frequency error is

$$\begin{aligned}
 \mathbf{Error}(t + \Delta t) &= \boldsymbol{\omega}(t + \Delta t) - \boldsymbol{\omega}_{\text{ref}0} \\
 &= (\mathbf{I} - \mathbf{T})^t \boldsymbol{\omega}(0) + \sum_{k=0}^{t-1} (\mathbf{I} - \mathbf{T})^k \mathbf{T} \boldsymbol{\omega}_{\text{ref}0} - \boldsymbol{\omega}_{\text{ref}0} \\
 &\quad + \sum_{k=0}^{t-1} (\mathbf{I} - \mathbf{T})^k \Delta t [\mathbf{R}_i(t - k\Delta t) + \mathbf{R}_o(t - k\Delta t)], \quad (29)
 \end{aligned}$$

where $\mathbf{T} = \Delta t (\mathbf{L} + \mathbf{G})$, the graph Laplacian matrix is $\mathbf{L} = \mathbf{D} - \mathbf{A}$, and the diagonal matrix of pinning gains is $\mathbf{G} = \text{diag}(g_i)$. The vectors $\mathbf{R}_i = [a_{ij} \times r_{ji}(t)]$ and $\mathbf{R}_o = [g_i \times r_{\text{ref},i}(t)]$ account for the system noise. Taking norm-two on both sides of (29) leads to

$$\begin{aligned}
 \|\mathbf{Error}(t + \Delta t)\| &= \|(\mathbf{I} - \mathbf{T})^t \boldsymbol{\omega}(0) + \sum_{k=0}^{t-1} (\mathbf{I} - \mathbf{T})^k \mathbf{T} \boldsymbol{\omega}_{\text{ref}0} \\
 &\quad - \boldsymbol{\omega}_{\text{ref}0} + \sum_{k=0}^{t-1} (\mathbf{I} - \mathbf{T})^k \Delta t [\mathbf{R}_i(t - k\Delta t) + \mathbf{R}_o(t - k\Delta t)]\| \\
 &\leq \|(\mathbf{I} - \mathbf{T})^t \boldsymbol{\omega}(0) + \sum_{k=0}^{t-1} (\mathbf{I} - \mathbf{T})^k \mathbf{T} \boldsymbol{\omega}_{\text{ref}0} - \boldsymbol{\omega}_{\text{ref}0}\| \\
 &\quad + \left\| \sum_{k=0}^{t-1} (\mathbf{I} - \mathbf{T})^k \Delta t \mathbf{R}_i(t - k\Delta t) \right\| \\
 &\quad + \left\| \sum_{k=0}^{t-1} (\mathbf{I} - \mathbf{T})^k \Delta t \mathbf{R}_o(t - k\Delta t) \right\|. \quad (30)
 \end{aligned}$$

By taking squares on both sides and expanding, we get (26). By considering expectation of the error, Since R_i and R_o are bounded and uncorrelated [20], the expectation of errors is given in (27). Taking the limit on both sides of (27) as $t \rightarrow \infty$, and since $\lim_{t \rightarrow \infty} (\mathbf{I} - \mathbf{T})^t = 0$ and $\lim_{t \rightarrow \infty} \sum_{k=0}^{t-1} (\mathbf{I} - \mathbf{T})^k \mathbf{T} \boldsymbol{\omega}_{\text{ref}0} = \boldsymbol{\omega}_{\text{ref}0}$, the mean-square deviation becomes

$$\begin{aligned}
 \lim_{t \rightarrow \infty} E[\|\mathbf{Error}(t + \Delta t)\|^2] &\leq \|\mathbf{T}^{-1} \Delta t\|^2 \|\mathbf{R}_{i,\text{max}}\|^2 \\
 &\quad + \|\mathbf{T}^{-1} \Delta t\|^2 \|\mathbf{R}_{o,\text{max}}\|^2 \\
 &\quad + 2\|\mathbf{T}^{-1} \Delta t\| \|\mathbf{R}_{i,\text{max}}\| \|\mathbf{T}^{-1} \Delta t\| \|\mathbf{R}_{o,\text{max}}\|. \quad (31)
 \end{aligned}$$

The upper bound for $\mathbf{R}_{i,\text{max}}$ can be obtained by using the maximum covariance of the noise associated with the neighboring communication links, $r_{i,\text{max}}$, and weights of the adjacency matrix, $\mathbf{R}_{i,\text{max}} = [a_{ij} \times r_{i,\text{max}}]$. In a practical setting, the covariance can usually be estimated based on the data available for different communication strategies [27]–[29]. It can be shown that \mathbf{R}_o is bounded ([20]-section 5.2). The expression for the upper bound of mean-square deviation

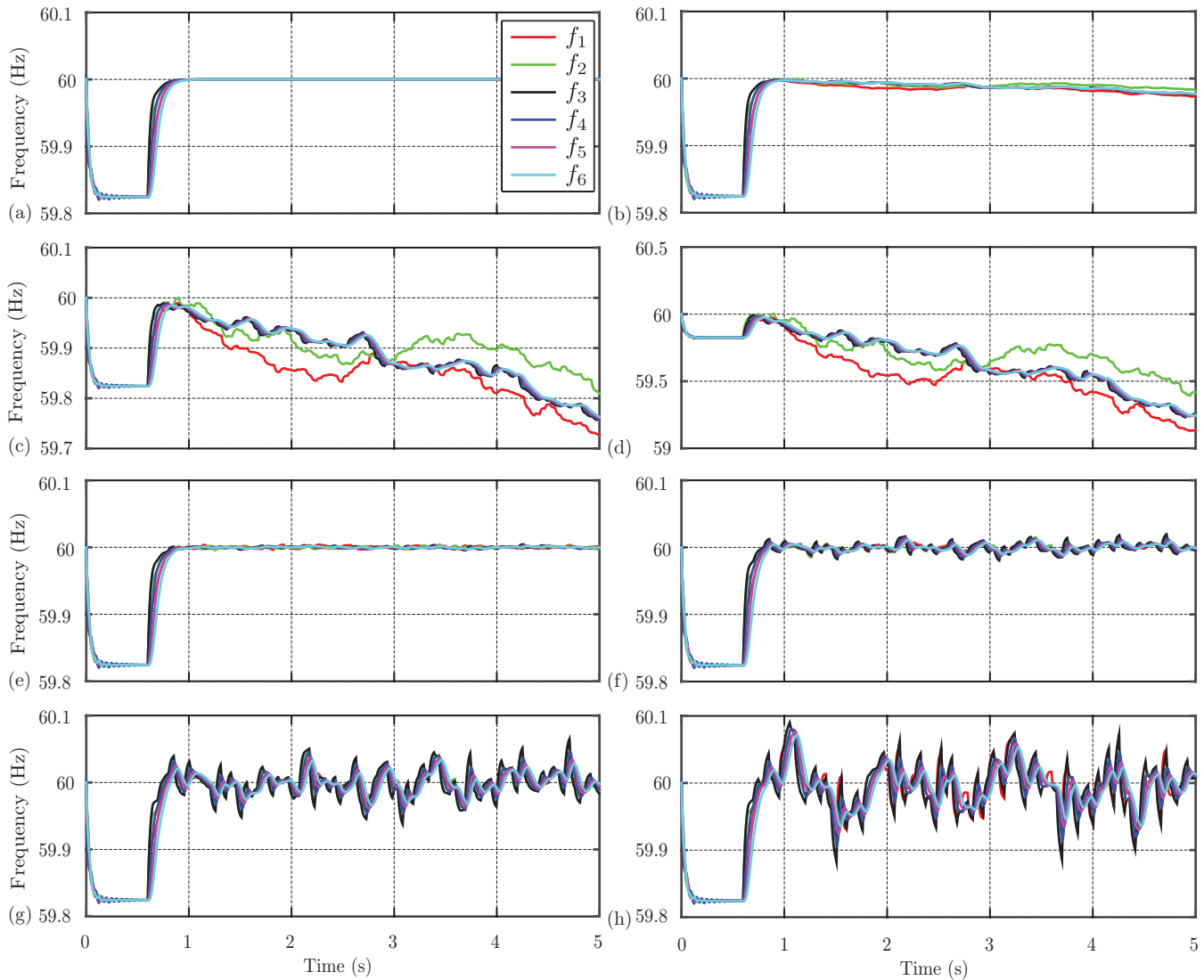


Fig. 5. Frequency synchronization in presence of noise: (a) Inverter frequencies under ideal conditions (no noise); (b) Inverter frequencies with noise $\sigma^2 = 10^{-4}$; (c) Inverter frequencies with noise $\sigma^2 = 10^{-2}$; (d) Inverter frequencies with noise $\sigma^2 = 0.1$; (e) Inverter frequencies with noise $\sigma^2 = 10^{-4}$ with DLMS algorithm; (f) Inverter frequencies with noise $\sigma^2 = 10^{-2}$ with DLMS algorithm; (g) Inverter frequencies with noise $\sigma^2 = 0.1$ with DLMS algorithm; (h) Inverter frequencies with noise $\sigma^2 = 0.1$ with DLMS algorithm, when the links between inverters 2 and 3 and the reference and inverter 2 fail.

for the DLMS algorithm, $\mathbf{R}_{o,\max}$, can be obtained similarly [20]. The upper bound on voltage error cannot be similarly defined since, as opposed to the frequency being a global variable which is consistent throughout the microgrid, inverter voltages should be different to allow reactive power sharing [9].

VI. CASE STUDIES

The performance of the proposed control method is evaluated for different noise levels in a communication network of an islanded microgrid. Figure 4 illustrates a single-line diagram of a modified 34-bus test feeder [30], augmented with six inverters. The feeder is connected to the main grid at bus 800. The feeder is converted to a balanced feeder by averaging the line parameters given in [30]. The load impedances are load 1 : $1.5 + j1 \Omega$, load 2 : $0.5 + j0.5 \Omega$, load 3 : $1 + j1 \Omega$, and load 4 : $0.8 + j0.8 \Omega$. The inverter specifications are

given in the Appendix. Each inverter is modeled by a 13-order dynamic system as described in (2), and the secondary control is implemented, in a distributed fashion, using (6) and (7). Loads have been modeled using a second-order dynamic model in (4). The nominal frequency and line-to-line voltage are 60 Hz and 24.9 kV, respectively. The inverters are connected to the feeder through Y-Y 480V/24.9 kV, 400 kVA transformers with a series impedance of $0.03 + j0.12$ p.u. Each inverter can communicate only with other inverters neighboring on a communication graph as shown in Fig. 4(a). Each inverter communicates its frequency, output voltage, estimated reference frequency, estimated reference voltage, and Lagrange multipliers to its neighbors. Inverters 1, 2, and 3 are pinned (receive reference signal) with pinning gains $g_1 = g_2 = g_3 = 1$. It is assumed that the noise in neighboring communication links and pinned reference links are the same.

The reference frequency and voltage for the secondary

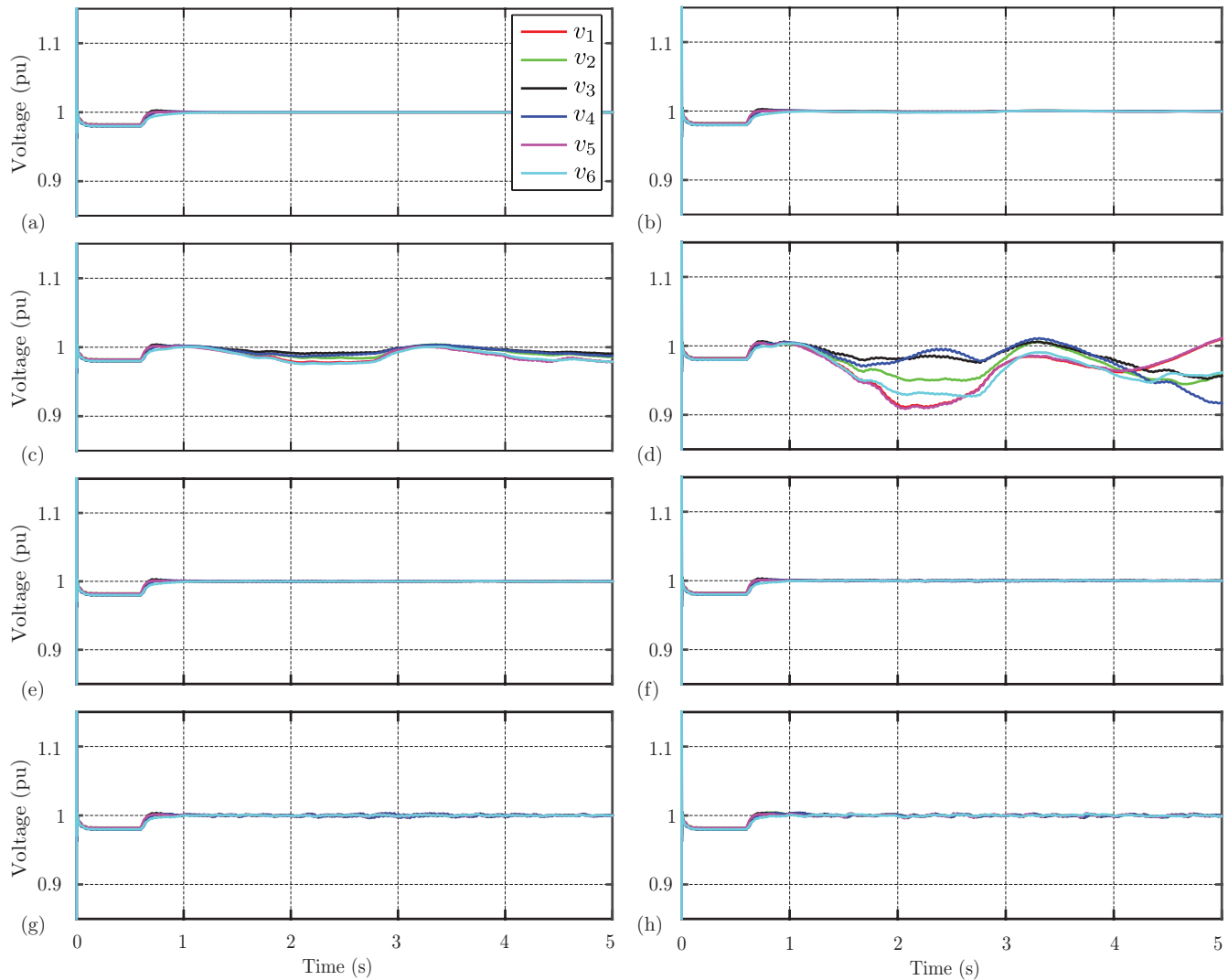


Fig. 6. Voltage synchronization in the presence of noise: (a) Inverter output voltage under ideal conditions (no noise); (b) Inverter output voltage with noise $\sigma^2 = 10^{-4}$; (c) Inverter output voltage with noise $\sigma^2 = 10^{-2}$; (d) Inverter output voltage with noise $\sigma^2 = 0.1$; (e) Inverter output voltage with noise $\sigma^2 = 10^{-4}$ with DLMS algorithm; (f) Inverter output voltage with noise $\sigma^2 = 10^{-2}$ with DLMS algorithm; (g) Inverter output voltage with noise $\sigma^2 = 0.1$ with DLMS algorithm; (h) Inverter output voltage with noise $\sigma^2 = 10^{-2}$ with DLMS algorithm, when the link failure occurs between inverter 2 and 3, and between the reference and inverter 2.

control are set to 60 Hz and 1 p.u., respectively. The test feeder is islanded from the main grid at $t = 0$ s. The cooperative secondary control is intentionally activated at $t = 0.7$ s. Under ideal conditions (no noise in the reference signal), as seen in Fig. 5(a) and Fig. 6(a), the frequency and voltage synchronize to the desired levels of $f = 60$ Hz and $V = 1$ p.u., respectively. Figures 5(b) and 5(c) show when reference links and communication links include noise with $\sigma^2 = 10^{-4}$ (variance) and $\sigma^2 = 10^{-2}$ respectively, the inverter frequencies do not synchronize in Fig. 5(c). The variance of $\sigma^2 = 10^{-2}$ implies a deviation of ± 0.3 Hz ($\pm 3\sigma$) in the frequency communicated. When the reference and communication links are corrupted with noises with $\sigma^2 = 0.1$, as seen in Fig. 5(d), the distortion in inverter frequencies increases even further.

Secondary frequency control is augmented with estimation as described in Algorithm 1, with $\mu = 0.05$. A similar strategy is adopted for the secondary voltage control. The inverter

frequencies, when embedded DLMS algorithms are considered in the secondary control, are shown in Figs. 5(e), (f), and (g) for noise levels of $\sigma^2 = 10^{-4}$, $\sigma^2 = 10^{-2}$, and $\sigma^2 = 0.1$, respectively. The inverter voltages are shown in Figs. 6(e), (f), and (g) for the noise levels of $\sigma^2 = 10^{-4}$, $\sigma^2 = 10^{-2}$, and $\sigma^2 = 0.1$, respectively. The inverter frequencies and voltages are synchronized within acceptable limits for the different noise levels. This is less effective for increased noise levels but, even for the noise level of $\sigma^2 = 0.1$, the frequencies and voltages are still within an acceptable range.

The performance of the proposed control algorithm augmented with estimation is studied under a link failure scenario in Figs. 5(h) and 6(h) with functioning links corrupted with noise signals with $\sigma^2 = 0.1$. Figures 5(h) and 6(h) show the output frequency and voltage when the link between inverters 2 and 3, and the link between the reference and inverter 2, fail. It can be seen that frequency and voltage terms synchronize

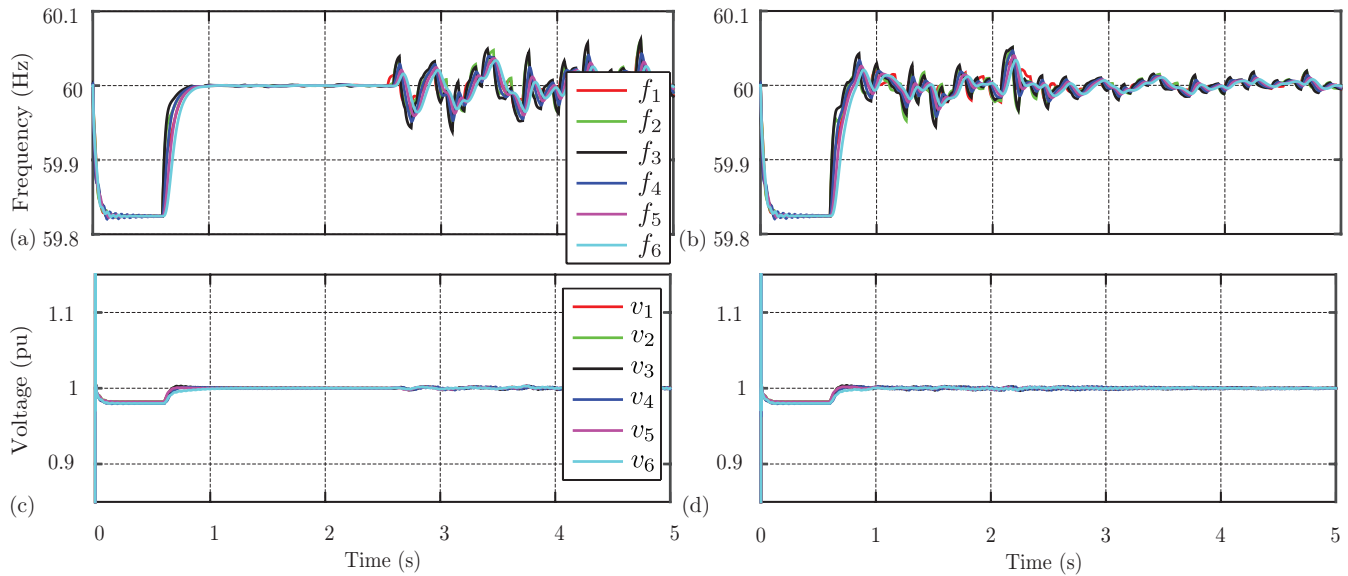


Fig. 7. Synchronization in the presence of varying noise levels: (a) Inverter frequencies when noise changes from $\sigma^2 = 10^{-4}$ to $\sigma^2 = 0.1$ at $t = 2.5$ s with DLMS algorithm ; (b) Inverter frequencies when noise changes from $\sigma^2 = 0.1$ to $\sigma^2 = 10^{-2}$ at $t = 2.5$ s with DLMS algorithm ; (c) Inverter output voltage when noise changes from $\sigma^2 = 10^{-4}$ to $\sigma^2 = 0.1$ at $t = 2.5$ s with DLMS algorithm ; (d) Inverter output voltage when noise changes from $\sigma^2 = 0.1$ to $\sigma^2 = 10^{-2}$ at $t = 2.5$ s with DLMS algorithm.

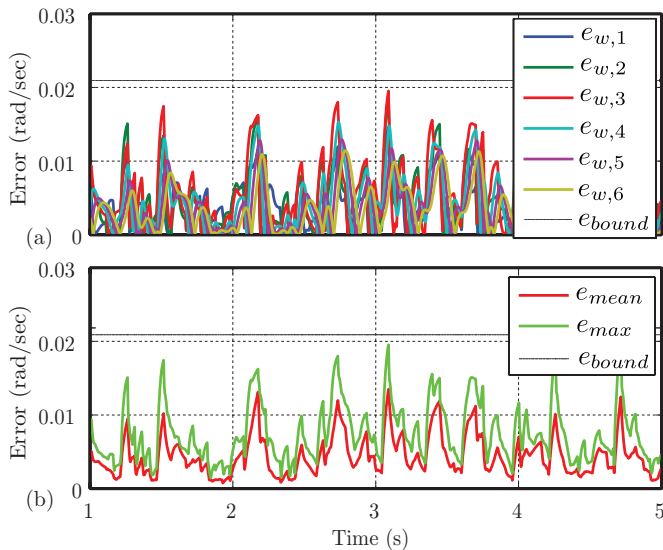


Fig. 8. Error levels in frequency terms: (a) Error in inverter frequencies with noise $\sigma^2 = 10^{-2}$; (b) Maximum and mean error with noise $\sigma^2 = 10^{-2}$. The theoretical upper error bound for the associated noise level is shown.

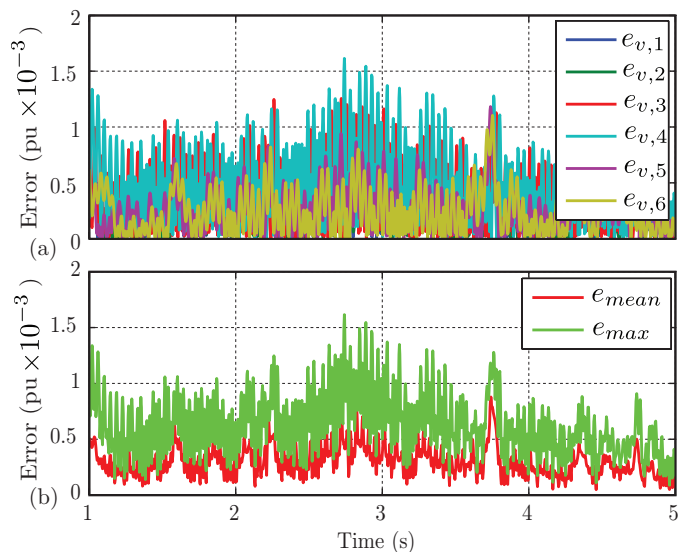


Fig. 9. Error levels in voltage terms: (a) Error in inverter's voltage with noise $\sigma^2 = 10^{-2}$; (b) Maximum and mean error with noise $\sigma^2 = 10^{-2}$.

given the presence of spanning tree in the communication graph topology, but the error due to noise is elevated but within acceptable limits. The controller performance, under various noise conditions, is studied in Fig. 7. Figures 7(a) and 7(c) show the output frequency and voltage when corrupted with noises with $\sigma^2 = 10^{-4}$ (variance) for $t < 2.5$ s, and $\sigma^2 = 0.1$ (variance) for $t > 2.5$ s. Figures 7(b) and 7(d) show the output frequency and voltage when corrupted with noises with $\sigma^2 = 0.1$ (variance) for $t < 2.5$ s, and $\sigma^2 = 10^{-2}$ (variance) for $t > 2.5$ s.

The upper error bound in frequency is calculated with

noise levels of $\sigma^2 = 10^{-2}$ in the reference and neighboring communication links. It is shown in Fig. 8 that the error in frequency obtained for each individual inverter is within the error bound derived in Section V. The microgrid system is simulated with 100 Monte Carlo runs and the error observed in frequencies is compared with the upper error bound in Fig. 8. The algorithm robustness can also be inferred as even with a variance $\sigma^2 = 10^{-2}$ indicating a deviation of ± 0.3 Hz, while the error is less than 0.03. The upper bound of voltage error cannot be similarly defined, as inverter voltages should be inherently different to ensure reactive power sharing. As seen from Fig. 9, the voltage deviations are also low. The error

in voltage and frequency for a noise level of $\sigma^2 = 10^{-2}$, observed in Figs. 6 and 8, respectively, is low and permissible in a practical scenario.

VII. CONCLUSION

This paper explores the noise-resilient synchronization of multi-inverter AC microgrids. The effect of different noise levels in the communication links on the secondary control of inverter frequency and voltage is evaluated. The performance of distributed noise reduction technique is evaluated for different noise levels in reference communication links and links connecting neighboring inverters. An expression for the upper error bound, due to the noise corruption, is derived. Error bound less than 0.03Hz for the communication noise deviation up to ± 0.3 Hz is verified using a modified 34-bus IEEE feeder test system.

APPENDIX

TABLE I
INVERTER SPECIFICATIONS

Output Connector	Inverter 1,2,4&5		Inverter 3&6	
	R_c	0.03 Ω	R_c	0.03 Ω
L_c	0.35mH	R_c	0.35mH	
LC Filter	R_f	0.1 Ω	R_f	0.1 Ω
	L_f	1.35mH	R_f	1.35mH
	C_f	50 μ F	R_f	50 μ F

TABLE II
CONTROLLER SPECIFICATIONS

Droop Gains	Inverter 1,2,4&5		Inverter 3&6	
	m_p	5.64×10^{-5}	m_p	7.5×10^{-5}
n_q	5.2×10^{-4}	n_q	6×10^{-4}	

REFERENCES

- [1] A. Bidram and A. Davoudi, "Hierarchical structure of microgrids control system," *IEEE Transactions on Smart Grid*, vol. 3, no. 4, pp. 1963–1976, Dec 2012.
- [2] D. Olivares, A. Mehrizi-Sani, A. Etemadi, C. Canizares, R. Iravani, M. Kazerani, A. Hajimiragha, O. Gomis-Bellmunt, M. Saeedifard, R. Palma-Behnke, G. Jimenez-Estevéz, and N. Hatziaargyriou, "Trends in microgrid control," *IEEE Transactions on Smart Grid*, vol. 5, no. 4, pp. 1905–1919, July 2014.
- [3] L. Che, M. Shahidehpour, A. Alabdulwahab, and Y. Al-Turki, "Hierarchical coordination of a community microgrid with AC and DC microgrids," *IEEE Transactions on Smart Grid*, vol. 6, no. 6, pp. 3042–3051, Nov 2015.
- [4] M. Savaghebi, A. Jalilian, J. Vasquez, and J. Guerrero, "Secondary control scheme for voltage unbalance compensation in an islanded droop-controlled microgrid," *IEEE Transactions on Smart Grid*, vol. 3, no. 2, pp. 797–807, June 2012.
- [5] A. Mehrizi-Sani and R. Iravani, "Constrained potential function-based control of microgrids for improved dynamic performance," *IEEE Transactions on Smart Grid*, vol. 3, no. 4, pp. 1885–1892, Dec 2012.
- [6] C. Ahumada, R. Cardenas, D. Saez, and J. Guerrero, "Secondary control strategies for frequency restoration in islanded microgrids with consideration of communication delays," *IEEE Transactions on Smart Grid*, 2015, to be published.
- [7] S. Cady, A. Dominguez-Garcia, and C. Hadjicostis, "A distributed generation control architecture for islanded AC microgrids," *IEEE Transactions on Control Systems Technology*, vol. 23, no. 5, pp. 1717–1735, Sept 2015.
- [8] A. Bidram, A. Davoudi, F. Lewis, and J. Guerrero, "Distributed cooperative secondary control of microgrids using feedback linearization," *IEEE Transactions on Power Systems*, vol. 28, no. 3, pp. 3462–3470, Aug 2013.
- [9] J. Simpson-Porco, Q. Shafiee, F. Dorfler, J. Vasquez, J. Guerrero, and F. Bullo, "Secondary frequency and voltage control of islanded microgrids via distributed averaging," *IEEE Transactions on Industrial Electronics*, vol. 62, no. 11, pp. 7025–7038, Nov 2015.
- [10] J. Schiffer, T. Seel, J. Raisch, and T. Sezi, "Voltage stability and reactive power sharing in inverter-based microgrids with consensus-based distributed voltage control," *IEEE Transactions on Control Systems Technology*, 2015, to be published.
- [11] F. Dorfler, J. Simpson-Porco, and F. Bullo, "Breaking the hierarchy: Distributed control & economic optimality in microgrids," *IEEE Transactions on Control of Network Systems*, 2015, to be published.
- [12] J. G. Proakis, *Digital Communications*. New York: McGraw-Hill, 1995.
- [13] L. Xiao, S. Boyd, and S.-J. Kim, "Distributed average consensus with least-mean-square deviation," *Journal of Parallel and Distributed Computing*, vol. 67, no. 1, pp. 33 – 46, Jan 2007.
- [14] M. A. Hanley, "Frequency instability problems in north american interconnections," National Energy Technology Laboratory Report, Tech. Rep. DOE/NETL-2011/1473, May 2011.
- [15] J. Hu and G. Feng, "Distributed tracking control of leader-follower multi-agent systems under noisy measurement," *Automatica*, vol. 46, no. 8, pp. 1382 – 1387, Aug 2010.
- [16] Y. Hong, G. Chen, and L. Bushnell, "Distributed observers design for leader-following control of multi-agent networks," *Automatica*, vol. 44, no. 3, pp. 846 – 850, March 2008.
- [17] L. Xiao and S. Boyd, "Fast linear iterations for distributed averaging," *Systems & Control Letters*, vol. 53, no. 1, pp. 65 – 78, Sep 2004.
- [18] F. Cattivelli and A. Sayed, "Diffusion LMS strategies for distributed estimation," *IEEE Transactions on Signal Processing*, vol. 58, no. 3, pp. 1035–1048, March 2010.
- [19] I. Schizas, G. Giannakis, S. Roumeliotis, and A. Ribeiro, "Consensus in ad hoc wsns with noisy links Part II: Distributed estimation and smoothing of random signals," *IEEE Transactions on Signal Processing*, vol. 56, no. 4, pp. 1650–1666, April 2008.
- [20] G. Mateos, I. D. Schizas, and G. B. Giannakis, "Performance analysis of the consensus-based distributed LMS algorithm," *EURASIP Journal on Advances in Signal Processing*, vol. 2009, no. 68, pp. 1–19, 2009.
- [21] S. Abhinav, I. Schizas, and A. Davoudi, "Noise-resilient synchrony of AC microgrids," in *Resilience Week (RWS)*, 2015, pp. 1–6.
- [22] R. Olfati-Saber and R. Murray, "Consensus problems in networks of agents with switching topology and time-delays," *IEEE Transactions on Automatic Control*, vol. 49, no. 9, pp. 1520–1533, Sept 2004.
- [23] N. Pogaku, M. Prodanovic, and T. Green, "Modeling, analysis and testing of autonomous operation of an inverter-based microgrid," *IEEE Transactions on Power Electronics*, vol. 22, no. 2, pp. 613–625, March 2007.
- [24] A. Bidram, F. Lewis, and A. Davoudi, "Distributed control systems for small-scale power networks: Using multiagent cooperative control theory," *IEEE Control Systems*, vol. 34, no. 6, pp. 56–77, Dec 2014.
- [25] R. G. Gallager, *Principles of digital communication*. Cambridge University Press, 2008.
- [26] D. P. Bertsekas and J. N. Tsitsiklis, *Parallel and Distributed Computation: Numerical Methods*. Prentice-Hall, Inc., 1989.
- [27] T. T. Cai, C.-H. Zhang, H. H. Zhou *et al.*, "Optimal rates of convergence for covariance matrix estimation," *The Annals of Statistics*, vol. 38, no. 4, pp. 2118–2144, 2010.
- [28] G. A. M. M. and G. L. Stuber, "Joint EM channel and covariance estimation with sufficient-statistic chip combining for a SIMO MC-CDMA antijam system," in *IEEE Wireless Communications and Networking Conference*, March 2008, pp. 1131–1136.
- [29] E. Conte, A. D. Maio, and G. Ricci, "Recursive estimation of the covariance matrix of a compound-gaussian process and its application to adaptive CFAR detection," *IEEE Transactions on Signal Processing*, vol. 50, no. 8, pp. 1908–1915, Aug 2002.
- [30] N. Mwakabuta and A. Sekar, "Comparative study of the IEEE 34 node test feeder under practical simplifications," in *39th North American Power Symposium*, 2007, pp. 484–491.